Nuclear Instruments and Methods in Physics Research 228 (1985) 259–266
North-Holland, Amsterdam

THE HHIRF SUPERSONIC GAS JET TARGET FACILITY

D. SHAPIRA, J.L.C. FORD, Jr. † and R. NOVOTNY *

*Oak Ridge National Laboratory **, Oak Ridge, Tennessee 37831, USA*

B. SHIVAKUMAR

*A.W Wright Nuclear Structure Laboratory ***, Yale University, New Haven, Connecticut 06520, USA and Oak Ridge National Laboratory, Oak Ridge, Tennessee 37831, USA*

R.L. PARKS + and S.T. THORNTON

Department of Physics ++, University of Virginia, Charlottesville, Virginia 22901, USA

Received 6 June 1984

We describe a supersonic gas jet target built for studying reactions induced by heavy ions with high energy resolution. The device produces very localized high density gas jets in a near vacuum environment and is presently installed in the scattering chamber of a magnetic spectrograph at the ORNL HHIRF. With a 100 MeV ^{16}O beam collimated to a size of approximately 1 mm^2 at the target, image sizes of 0.42 mm have been obtained at the focal plane of the spectrograph with a solid angle of 2.4 msr and target densities of 15–30 $\mu g/cm^2$.

1. Introduction

Most requirements for high resolution studies of heavy ion induced reactions can be met by using windowless gas targets [1]. Clean (no carbon buildup), uniform and nondestructible pure targets of variable thickness can be produced. The absence of entrance and exit foils minimizes energy straggling and makes the bombardment with heavy ion beams of high intensity possible. Two serious drawbacks of differentially pumped gaseous targets are the low densities achievable in the central target region and the nonlocalization of the gaseous region.

Some of the more commonly used techniques for obtaining high resolution data with heavy ion induced reactions involve kinematic coincidence measurements with precise angle determination [2] or the use of magnetic spectrographs which compensate for the large spread in momentum for heavy products emitted over a finite angular range [3]. Both techniques require a well localized and small reaction region. A high density supersonic jet of gas can be configured to emulate a thin target foil [4]. Such a device has the advantages of a differentially pumped windowless gas target and in addition is highly localized. These obvious advantages have prompted several investigators to develop gas jet targets for use in heavy ion reaction studies [4–7] as well as for light ion studies where high target purity and density are needed [8].

This publication describes the supersonic gas jet target facility built at HHIRF. The target assembly has been designed to be portable except for the large vacuum pumps for the first stage. The use of the gas jet target in conjunction with a magnetic spectrograph tests the high resolution capabilities of both target and spectrograph. Actual measurements have shown that high resolution operation is easily accomplished. Following a brief description of the device, test results and samples of data will be given.

† Deceased.

* Present address: 2nd Physics Institute, University of Giessen, D-6300 Giessen, Fed. Rep. Germany.

** Operated by Martin Marietta Energy Systems, Inc. under contract DE-AC05-84OR21400 with the U.S. Department of Energy.

*** Supported by the U.S. Department of Energy under contract AC02-70ER03074.

+ Present address: E Systems, 7700 Arlington, Blvd., Falls Church, Virginia 22046, USA.

++ Supported in part by the National Science Foundation.

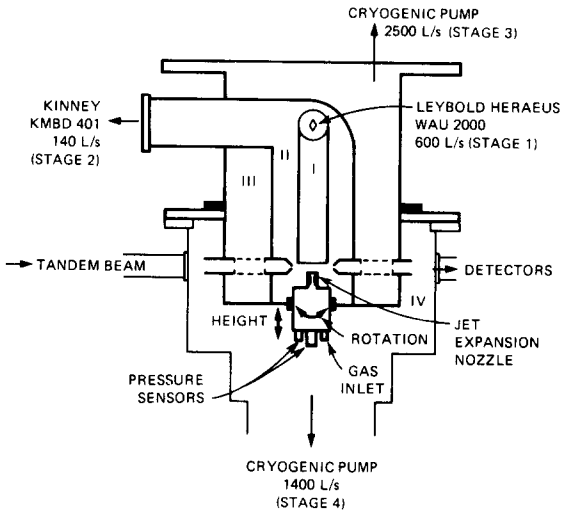

Fig. 1. Schematic view of gas jet device. The central part (heavier line) may be removed as one unit and can fit in a different chamber. The four different stages of the vacuum system and their pumps are indicated. The gas flows upward from the jet.

2. Description of the gas jet target

The essential features of our design appear in figs. 1 and 2 which show two schematic views of the apparatus (the mechanical details have been omitted for the sake of clarity). At the center and the heart of this device is a convergent–divergent laval nozzle [9] which allows for rapid supersonic expansion of gas at high pressures into the target region. In this device the gas moves upward, and close above the nozzle is an intake tube through which more than 90% of the gas flowing out of the laval nozzle is pumped away (stage I). Surrounding this central region are three additional stages of differential pumping, the last of which (stage IV) is the chamber into which the gas jet has been mounted. The parts of the gas jet drawn in heavy lines in fig. 1 can be removed as an unit and mounted at other sites.

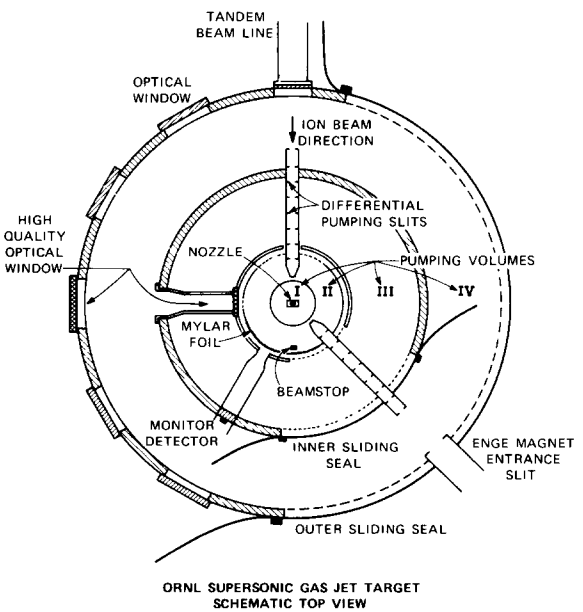

Fig. 2. Horizontal cutaway view of gas jet. Note that volumes II, III and IV are connected only through differential pumping slits which are needed for beam entrance and reaction product exit.

2.1. Vacuum system and gas flow control

The identification of the vacuum pumps and the pumping speeds of the vacuum pumps used in the present setup are indicated in fig. 1. Additional information on the gas pressures in the different stages are listed in table 1 for a variety of operating parameters. About 90% of the gas is pumped away in stage I and most of the remainder in stage II leaving less than 1% of the gas for stages III and IV. In the plan view of the apparatus shown in fig. 2, differential pumping apertures separate vacuum regions II, III, IV. This allows a great reduction in the pumping loads on stages III and IV to levels where cryogenic pumps can be used. The gas can easily be recycled from the outputs of the mechanical pumps used for stages I and II. Provision for recapturing and cleaning the gas to be reused has been provided, but has not yet been used.

A schematic drawing of the gas handling system used to control gas flow through the jet is shown in fig. 3. For normal operation only one control stage is needed (by-pass valve B2 can be left open); the pressure P_0 is then controlled by C1. Both controls are needed when operating the gas jet in a recycling mode. This permits us to run at inlet presurres P_0 that may not be compatible with the pressure that is optimal for the recycling line (near one atmosphere). The electronic pressure/flow control system consists of MKS Baratron, pressure

Table 1
Typical target densities and gas pressures in the different pumping stages for nitrogren gas.

P_0 Torr: $\times 1$	P_I $\times 10^{-3}$	P_{II} $\times 10^{-3}$	P_{III} $\times 10^{-4}$	P_{IV} $\times 10^{-6}$	Target thickness (10^{18} at./cm^2)
100	200	60	1.2	1.2	0.231
200	543	90	1.8	1.4	0.462
300	779	130	2.2	2.1	0.693
400	985	190	2.6	2.8	0.924
500	1186	250	3.2	3.1	1.155
600	1381	350	3.9	3.4	1.386

During these measurements the pressure in the beam line remained below 3×10^{-8} Torr.

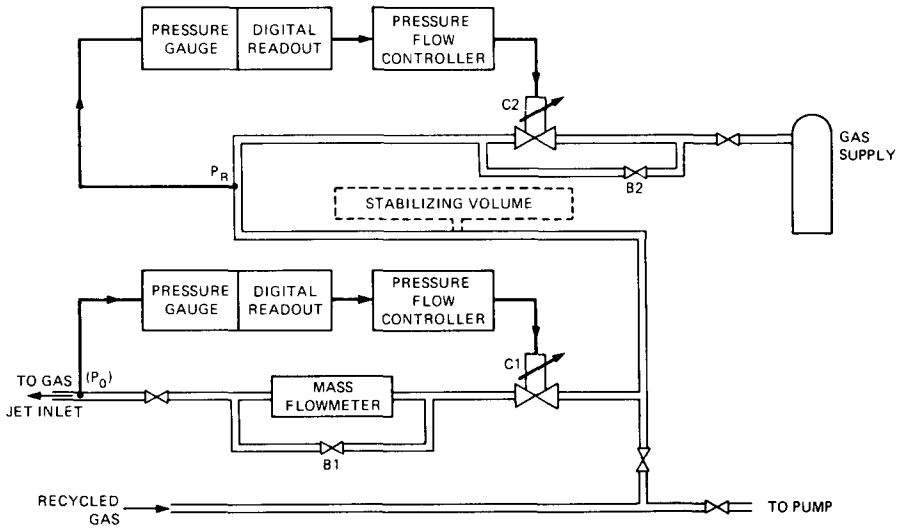

Fig. 3. Schematic drawing of gas handling system.

gauges model no. 220B, digital readout units MKS 200-PDR-C-2, MKS 250B pressure/flow controllers, a 248A-V-20000 SCCM valve (C2), and an MKS-251-5000 SCCM valve (C1).

2.2. Nozzle Design

The type of laval nozzle that we use is shown in fig. 4. It was designed to provide a thin sheet of dense gas, closely resembling a solid target. The formulae that describe supersonic jet flow [9,10] are based on the treatment of gas flow in two dimensions. Fig. 5 shows the predicted shape of the gas jet and a list of several parameters for an idealized situation of a jet propagating into an absolute vacuum. The formulae on which these predictions are based appear in appendix A and were taken from ref. [9]. In the actual and nonideal situation the jet propagates into a region where there is residual gas. The traingular tongue that protrudes from the nozzle's mouth becomes elongated and its boundaries curve in actual use. The properties of such nonideal jets have been widely discussed in the literature [10]. The parameters of the gas jet can be predicted with considerable accuracy near the nozzle exit at the first high density knot region. We have opted to use this region as the target, which obviates the need for any online di-

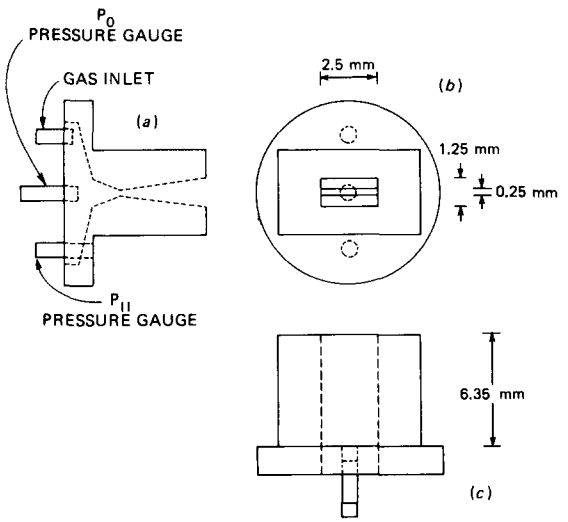

Fig. 4. Three views of the expansion nozzle used for forming the supersonic jet.

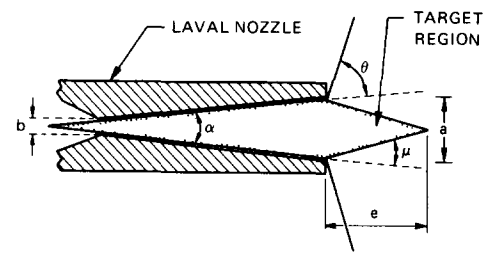

SUPERSONIC GAS JET FLOW PARAMETERS

GAS	MACH NO. M	θ (deg)	μ (deg)	TARGET HEIGHT e (mm)	MASS FLOW RATE M (g/s)	TARGET THICKNESS t ($\mu g/cm^2$)
N_2	3.17	77.43	18.36	2.25	0.214	14.19
Ar	3 8	41.76	15.26	2.83	0.262	21.27

Fig. 5. The shape of the gas jet and several jet parameters. The data indicate the gaseous region.

agnostics that would have been necessary if we had used one of the secondary high density knots downstream as the target.

Conditions at the first knot depend to first order only on the status of the gas at the inlet (pressure P_0 and temperature) and the physical dimensions of the nozzle. A tightly collimated beam interacts with the target as close as possible above the nozzle's exit. External vertical positioning of the nozzle allows precise positioning of the nozzle with respect to the beam.

2.3. Beam entrance and exit systems

Because of the shape of the jet (see fig. 5) it is clear that uniform target thickness can be maintained only with a small beam spot. The differential pumping apertures between regions II, III and IV for both the beam entrance and reaction products exit, only allow a useful target area less than 2×2 mm^2.

The reaction products exit port is mounted on a sliding seal and its motion is presently restricted to a laboratory angular range between 0° and 60°. This arrangement makes coincidence experiments difficult although we do have a fixed solid state detector at an angle of 45° separated from the vacuum (region III) by a thin mylar foil (see fig. 2). The effective solid angle was derived from the aperture's geometry. It was also determined by measuring the rate of α-particles reaching a detector positioned behind the aperture, from an emitter of known activity, placed and moved about the target center position.

The collimation system used in front of the scattering chamber for the gas jet beam line is an important ingredient of the system and is shown together with the rest of the magnetic spectrograph–detector system in fig. 6. The degree of collimation varies from one experiment to another but in general at least two of the three defining slits (S_1, S_2 and A) are narrowed down to approximately 1 mm opening size. Typical beam transmission ratios of about 30% have been obtained under these conditions.

As is apparent from fig. 2, the beam itself is stopped inside the gas jet apparatus which serves as a Faraday cup. The whole device is isolated from ground and the differential pumping slits at the entrance are large enough to transmit the beam unscathed ensuring that all the beam charge collected has also passed through the target region. We have run numerous tests which indicate that the beam charge integral does indeed yield the total number of particles incident on the target. These measurements have shown that tight collimation of the beam prior to entering the gas jet apparatus is needed to allow for correct charge integration. The collimating slits (S_1, S_2, and A in fig. 6) are located 1.7, 0.9 and 0.7 m upstream, respectively, and an electron suppression ring has been installed just in front of the entrance to the scattering chamber.

3. Gas jet operation and testing

Absolute cross section measurements can be performed with such a device provided that one can obtain reliable data on the product of beam fluence and target atom density. The target density and the beam fluence can be obtained separately. The total charge collected coupled with knowledge of the beam's charge state and proper collimation of the beam yield the fluence of incident particles.

In order to estimate the target density one has to rely on theoretical predictions for gas jet propagation [9,10]. These are readily available in particularly simple form for the first high density knot close to the nozzle's exit. Fig. 7 shows target areal densities of a N_2 gas target

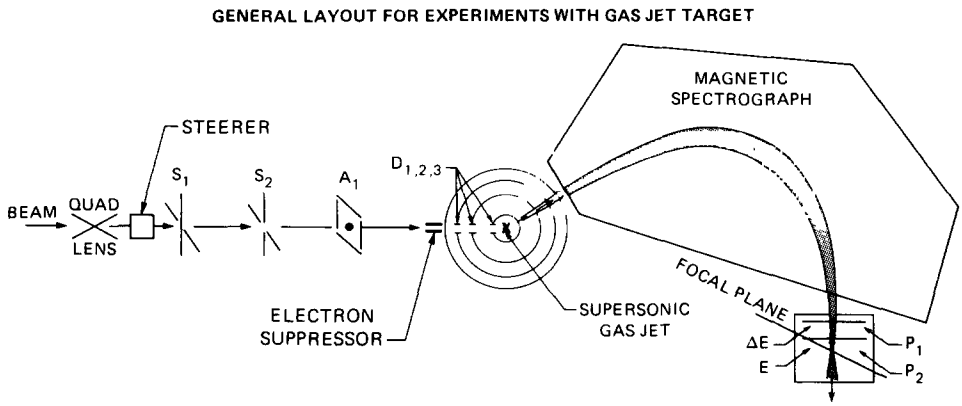

Fig. 6. The general layout of the gas jet beam line and data taking system. S_1 and S_2 are two four-jaw slits with current read out. A_1 is a circular aperture and $D_{1,2,3}$ are the differential pumping slits.

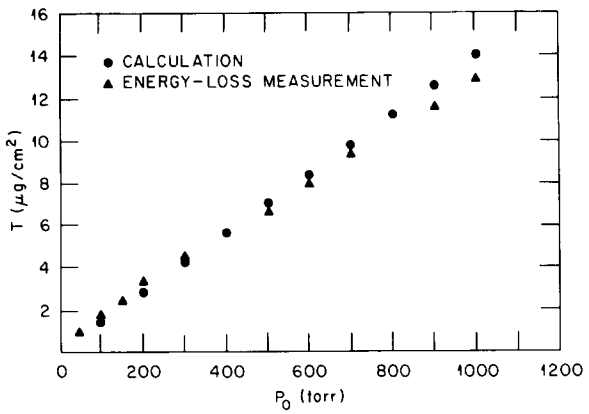

Fig. 7. The variation of target thickness as a function of inlet pressure. Shown are target thicknesses determined experimentally (triangles) by measuring the energy loss of 12 MeV ^{16}O in the target gas and also calculated values.

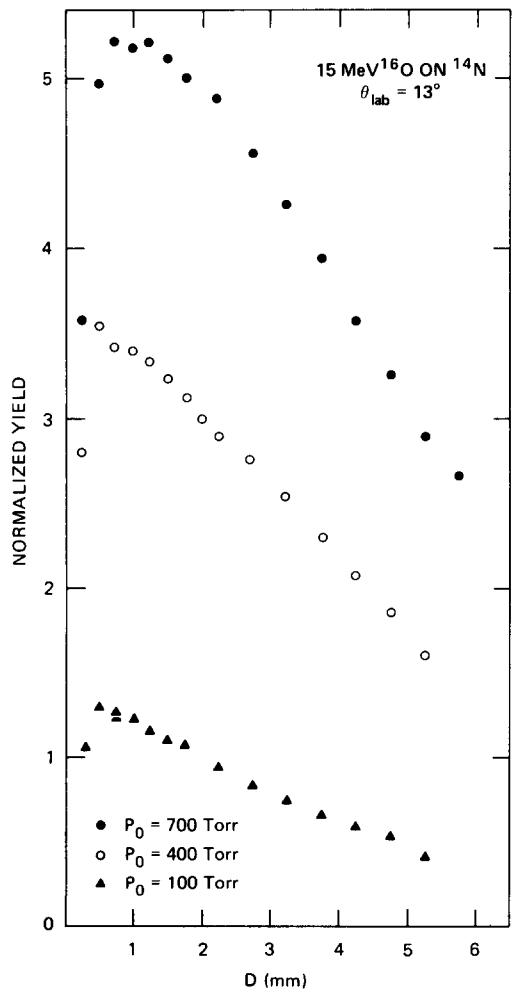

Fig. 8. Gas jet profile measurements. These data correspond to target thickness as a function of distance from the jets exit aperture.

calculated with the formulae that appear in appendix A for various inlet pressures. These predictions are compared to measusred target thicknesses data (fig. 7) which were obtained by measuring the energy loss of 12 MeV $^{16}O^{3+}$ ions scattered by the gas jet target. Additional tests were run comparing measured cross sections at low bombarding energies with Rutherford scattering – these tests, however, probe the product of target density and total incident beam. An additional normalization method involves the direct determinaton of the product of target density and beam fluence. A small but predetermined amount of xenon gas is mixed with the target gases used in the experiment. The comparison of the elastic yield from both xenon and the target gas provides a method for absolute normalization of the reaction data provided that the scattering of the same beam from ^{132}Xe is Rutherford scattering. This method has been used successfully with a gas cell target [11]. The energy loss measurements and Rutherford cross section measurements have shown good agreement both in shape and magnitude with the calculations (see fig. 7) when the beam was properly collimated.

The actual shape of the jet has been investigated by rotating the nozzle at an angle with respect to the beam and by moving the nozzle up and down with respect to the beam. The normalized yield for scattering of 15 MeV ^{16}O from a ^{14}N jet was measured at a scattering angle of 13° in the lab, as a function of the laval nozzle's height with respect to the beam for three different target densities. The resulting profiles shown in fig. 8 agree with the trend shown in fig. 5, although the high density region of the jet is somewhat longer as expected.

4. Data samples and evaluation

As shown in fig. 6 the detection system includes a trajectory sensitive detector at the focal plane of a magnetic spectrograph. This detector is capable of measuring the total energy, energy loss and two position signals along the focal plane region for incident ions [12]. A final test of the system was made with a study of peripheral reactions induced by 100 MeV ^{16}O on ^{40}Ar. The target consisted of a jet of natural argon gas (99.6% ^{40}Ar) with areal density of 15 $\mu g/cm^2$. A solid angle of 2.4 msr (2.5° opening) and incident beam intensities of 10 particle nA. The simultaneous and independent measurements of energy and momentum of the outgoing products enabled us to separate the different masses of the outgoing products. Fig. 9 shows a two-dimensinal scatter plot made for outgoing oxygen ions detected in the focal plane of the magnetic spectrograph, and fig. 10 provides a one-dimensional projection on the focal plane for the outgoing ^{17}O nuclei. The different excited states in ^{39}Ar are identified and the energy resolution attained here is about 100 keV (one part in 10^3). Using the

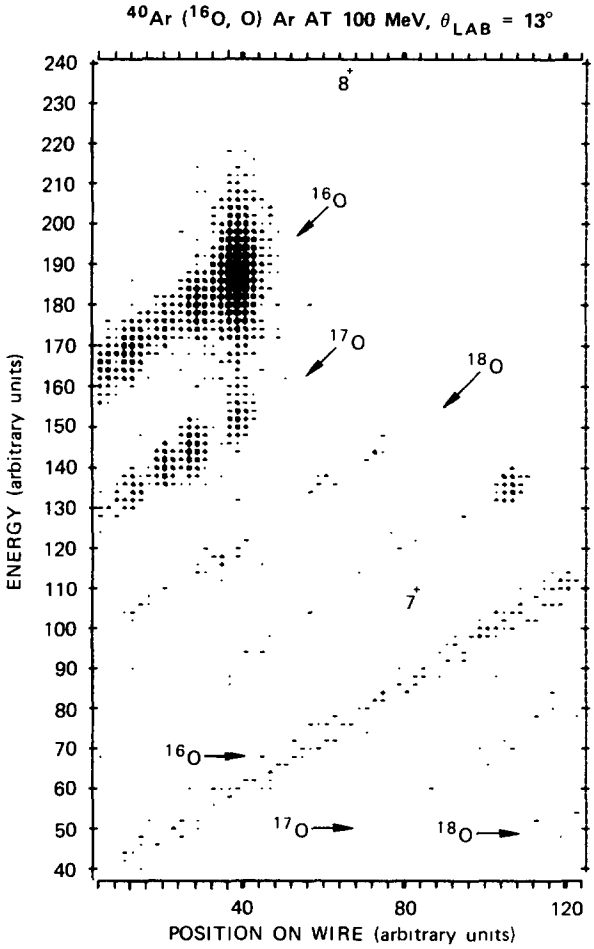

Fig. 9. An energy vs focal plane position (momentum) plot of outgoing products with $Z = 8$ (oxygen) from the reactions of ^{16}O with ^{40}Ar. Oxygen ions with charge states of 7^+ and 8^+ are observed.

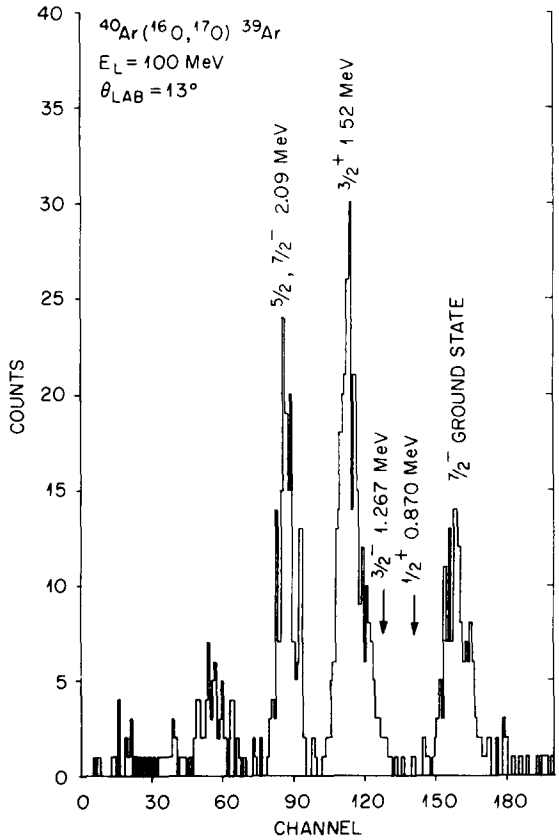

Fig. 10. A projected momentum spectrum of outgoing ^{17}O from fig. 9. The excited states of ^{39}Ar are shown there and an overall energy resolution of ~ 100 keV is obtained.

integrated charge collected we were able to determine the elastic angular distribution. The elastic scattering data for $^{16}O + ^{40}Ar$ are shown in fig. 11. There are no elastic data available with which to compare these results, but the results look perfectly reasonable (the estimated grazing angle is about 17.5°).

The spectrum shown in fig. 10 corresponding to a position resolution along the focal plane of about 1.5 mm. this spectrum was obtained by ray tracing to the focal plane using the position information from two position sensitive wires. With an object size of about 1.2 mm (the width of the nozzle's exit) images sizes of 0.4 mm should be possible because the magnetic spectrograph has a horizontal demagnification factor of about 3. We concluded that the resolution was not limited by focussing on the magnet but by the inherent position resolution of the two wire counters (~ 1 mm). The elastic scattering of 100 MeV ^{16}O from ^{40}Ar was there-

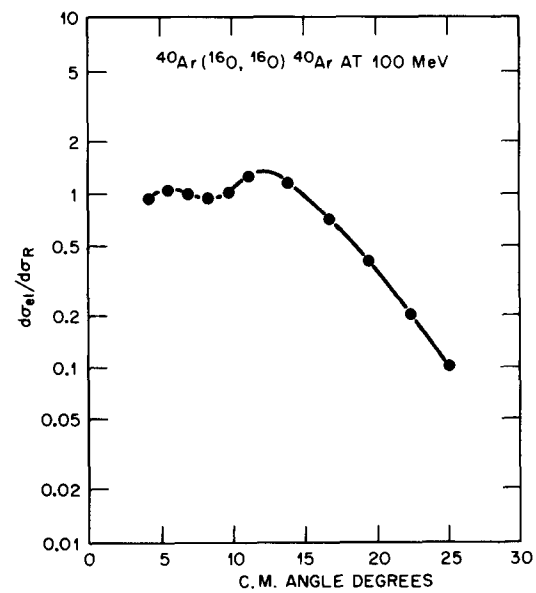

Fig. 11. Elastic scattering of $^{16}O + ^{40}Ar$.

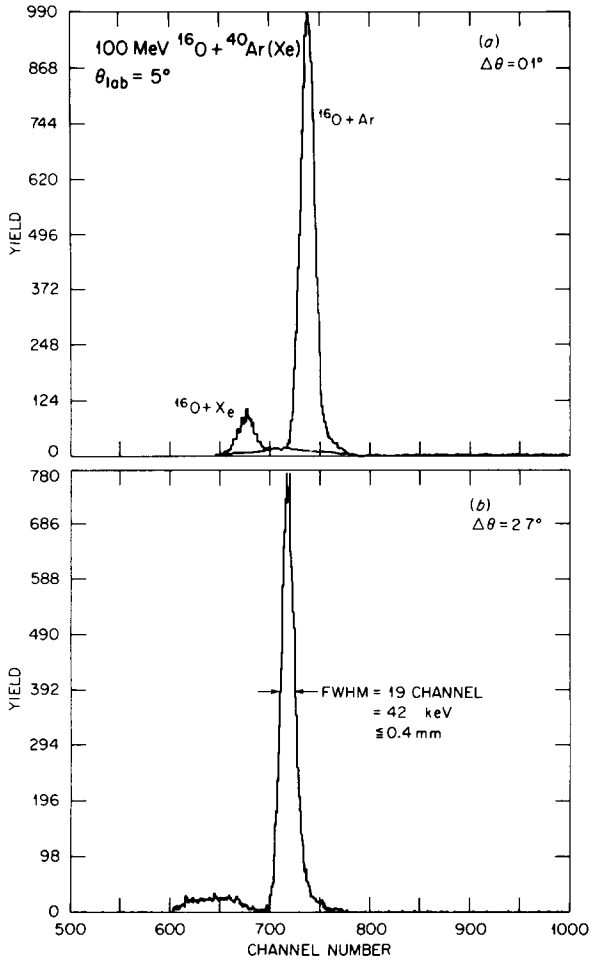

Fig. 12. High resolution position spectra for the elastic scattering of ^{16}O on a mixture of ^{40}Ar and Xe. The width of the $^{16}O + Ar$ peaks correspond to a position resolution of 0.4 mm. In part (*a*) both the $^{16}O + Ar$ and the $^{16}O + Xe$ elastic scattering peaks appear narrow because with a small acceptance angle no focusing is required to obtain good resolution.

fore remeasured using a solid state position sensitive detector. The resulting position spectrum that we obtain appears in fig. 12. It shows a focused peak for $^{16}O + ^{40}Ar$ elastic scattering and also, nearby, the $^{16}O + Xe$ elastic peak which clearly is not focused on the same plane. The data shown here were taken with a 5 $\mu g/cm^2$ target and a solid angle of 2.4 msr for a lab angle of 5°. The observed focusing to a ~ 0.4 mm spot size, which corresponds to the counter's resolving power, demonstrates that the object size indeed does not exceed 1.2 mm. We obtain these resolution results independent of the solid angle acceptance of the spectrograph as evidenced in fig. 12 by the two values of $\Delta\theta$. These data demonstrate that when coupled with a high resolution

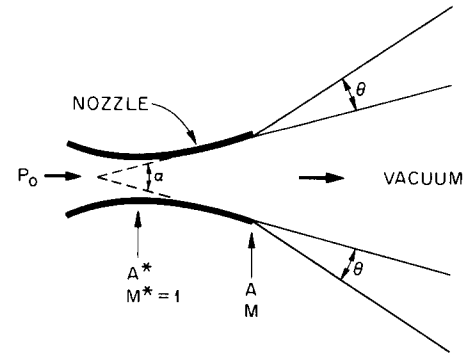

Fig. 13. Supersonic gas flow through a laval nozzle.

position-sensitive detector this system is capable of momentum resolution better than 5 parts in 10^4 for heavy ion raction studies.

A recirculating gas handling system is presently under construction, and we estimate that about 10 liter atmospheres of gas would be sufficient to operate the gas jet target in a closed loop recylcing mode. Provisions are also being made to upgrade the apparatus for targets of high temperature seeded jets and vapors.

We gratefully acknowledge the assitance of S. Suwana-adth in the early stages of construction and testing of the gas jet apparatus.

Appendix A

Supersonic nozzle flow

Notation (see fig. 13)

P_0, V_0, T_0, ρ_0 – stagnation volume variables
P^*, V^*, T^*, ρ^* – nozzle throat variables
P, V, T, ρ – nozzle exit variables
A^* – nozzle throat area
A – nozzle area upstream.

Gas constants

$\gamma \equiv \frac{C_P}{C_V}$ $\quad \alpha \equiv (1 + \frac{\gamma - 1}{2} M^2)$
$M \equiv q/a$ $\quad a$ – velocity of sound
q – gas velocity
$\therefore M \equiv$ Mach number.

Assumptions

Assume an incompressible ideal gas undergoing adiabatic expansion.

(A) $qA\rho = \text{const}$ (incompressible)
(B) $P = \rho RT$ (ideal)
(C) $a^2 = \gamma RT$ (adiabatic process).

When P_0/P^* becomes larger than a critical ratio, gas flow through the throat will be at sound velocity, i.e., $M^* = 1$. From there on gas flow becomes supersonic and the velocity past the nozzle throat depends only on the cross section of the nozzle:

1) $$\frac{A}{A^*} = \frac{1}{M}\left(\left(\alpha(M)/\left(\frac{\gamma+1}{2}\right)\right)^{(1/2)(\gamma+1)/(\gamma-1)}\right)$$

(for $M^* = 1$). Also

2a) $T/T_0 = 1/\alpha$,

2b) $\rho/\rho_0 = (1/\alpha)^{1/(\gamma-1)}$ and

2c) $P/P_0 = (1/\alpha)^{\gamma/(\gamma-1)}$.

Mass flow (g/s):

3) $$m = \sqrt{\gamma}\left(\frac{\gamma+1}{2}\right)^{-(1/2)(\gamma+1)/(\gamma-1)}\sqrt{P_0\rho_0}\,A^*.$$

Deflection angle of gas flow:

$$\omega(M=1) = 0,$$

$$\omega(M) - \omega(1) = \sqrt{\frac{\gamma+1}{\gamma-1}}\,\tan^{-1}\sqrt{\frac{\gamma-1}{\gamma+1}(M^2-1)} - \tan^{-1}\sqrt{M^2-1},$$

$$\omega(M=\infty) \equiv \omega_{\max} = \frac{\pi}{2}\left[\sqrt{\frac{\gamma+1}{\gamma-1}} - 1\right].$$

The deflection angle in the gas flow as it leaves the nozzle and expands into perfect vacuum is therefore given by

$$\theta = \omega_{\max} - \omega(M),$$

$$\therefore \theta = -\frac{\pi}{2} + \tan^{-1}\sqrt{M^2-1} + \sqrt{\frac{\gamma+1}{\gamma-1}}\left[\frac{\pi}{2} - \tan^{-1}\sqrt{\frac{\gamma-1}{\gamma+1}(M^2-1)}\right].$$

References

[1] W. Del Bianco and G. Kajrys, Nucl. Instr. and Meth. 204 (1983) 289 and references therein,
C. Rolfs, J. Gorres, K.U. Kettner, H. Lorenz-Wirzba, P. Schalbrock, H.P. Trautvetter and W. Verhoeven, Nucl Instr. and Meth. 157 (1978) 19;
K.W. Allen et al., Nucl. Instr. and Meth. 134 (1976) 1;
J. Brussiere and J.M. Robson, Nucl. Instr. and Meth. 91 (1971) 103;
C.M. Jones, J.W. Johnson and R.M. Beckers, Nucl. Instr. and Meth. 68 (1969) 337.

[2] H. Emling, R. Novotny, D. Pelte and G. Schreider, Nucl. Phys. A211 (1973) 600.

[3] T. Walcher, Magnetic spectrographs for the investigation of heavy ion reactions in experimental methods in heavy ion physics, Lecture notes in physics, no. 83 (Springer Verlag, Berlin, 1980).

[4] R. Beringer and W. Wall, Rev. Sci. Instr. 28 (1957) 77.
J. Ulbright, G. Clausnitzer and G. Graw, Nucl. Instr. and Meth. 102 (1972) 93.
D.A. Gross and A. Melissinos, Nucl. Instr. and Meth. 130 (1975) 1.

[5] W. Tietsch, K. Bethge, H. Feist and E. Schopper, Nucl. Instr. and Meth. 158 (1979) 41.

[6] M. Treichel, R. Isenbugel and N. Marquardt, Nucl. Instr. and Meth. 212 (1983) 101.

[7] H.W. Becker, L. Buchman, J. Görres, K.U. Kettner, H. Krawinkel, C. Rolfs, P. Schmalbrock, H.P. Trautvetter and A. Vlieks, Nucl. Instr. and Meth. 198 (1982) 277.

[8] G. Bittner, W. Kretchmer and W. Schuster, Nucl. Instr. and Meth. 161 (1979) 1.

[9] J.A.D. Ackroyd, SRC Daresbury Report DL/NSF/R12 (1975) unpublished.

[10] T.C. Adamson, Jr. and J.A. Nicholls, J. Aerospace Sci. 26 (1959) 16;
S. Crist, P.M. Sherman and D.R. Glass, AIAA J. 4 (1966) 68.

[11] D. Shapira, R.A. Dayras, J.L.C. Ford, Jr., J. Gomez del Campo, A.H. Snell, P.H. Stelson and R.G. Stockstad, Nucl. Instr. and Meth. 163 (1979) 325;
D. Shapira et al., Phys. Rev. C 28 (1983) 1148.

[12] D. Shapira, G. Bomar, J.L.C. Ford, J. Gomez del Campo and L.C. Dennis, Nucl. Instr. and Meth. 169 (1980) 77.